Available on CMS information server

CMS NOTE-2008/006

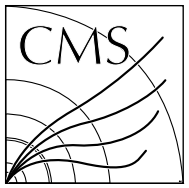

The Compact Muon Solenoid Experiment

CMS Note

Mailing address: CMS CERN, CH-1211 GENEVA 23, Switzerland

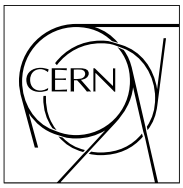

18 September 2007

Determination of the Lorentz Angle in Microstrip Silicon Detectors with Cosmic Muons

V. Ciulli, R. D'Alessandro, S. Frosali, C. Genta

Abstract

The microstrip silicon tracker of the CMS experiment will operate in a 4 T magnetic field in the harsh radiation environment of the Large Hadron Collider. The drift motion of the charge carriers will be therefore affected by the Lorentz force due to the high magnetic field. Furthermore, radiation damage will change in time the properties of this drift. In this note a method to measure the Lorentz angle from reconstructed tracks is presented and results obtained on Magnet Test and Cosmic Challenge data are compared to the values expected from a model, developed by the authors, which takes into account all the relevant parameters during the tracker lifetime (e.g. temperature and depletion voltage of the detectors).

1 Introduction

The Lorentz angle Θ_L, by which charge carriers in a silicon sensor are deflected in a magnetic field B transverse to the drift direction, is given by

$$\tan\Theta_L = \mu_H B = r_H \mu B\,, \tag{1}$$

where, the Hall mobility μ_H is the drift mobility in a magnetic field. This is related to the mobility without magnetic field μ by the Hall factor r_H, which has a value of ≈ 0.7 for holes and ≈ 1.15 for electrons [1]. For the CMS microstrip silicon tracker only the drift of the holes is important, since they are the charge carriers collected on the sensor strips [2]. Because of the Lorentz force, the 4T magnetic field inside CMS causes a significant shift of the holes during their motion. Thus a correction must be applied to the reconstructed hit positions. Any error in the assumed Lorentz angle would result in an apparent misalignment of the silicon sensors. In particular, the effect of the high irradiation doses in the Large Hadron Collider environment will change the drift properties in the silicon and may affect the Lorentz angle too.

In the summer of 2006, the CMS collaboration took advantage of the magnet commissioning tests and of the partial installation of some of the subdetectors in the above ground hall to do the Magnet Test and Cosmic Challenge (MTCC) [3]. At the MTCC, a fraction of all subdetectors (with the exception of the pixel systems) was operated with an up-to 4 T magnetic field delivered by the superconducting solenoid and read out with a downscaled final-design global data acquisition system (DAQ). Cosmic muon triggering was provided by the Level-1 trigger electronics of the muon detectors.

Despite the fact that the MTCC tracker setup represented only about 1% of the final system, most of the selected hardware and software components were prototypes of the final versions. The MTCC, therefore, offered the unique opportunity of testing the performance of the tracker in the presence of the 4 T magnetic field and the Lorentz angle is among the most interesting parameters to have been measured.

The note is organized as follows. In the first part an estimate of the Lorentz angle in silicon detectors is obtained from a model for the drift of the holes. Then the measurement of the Lorentz angle on MTCC data is presented and results are compared to the expectations.

2 Prediction of Lorentz angle at MTCC

For the calculation of the hole deviation from its normal motion due to the Lorentz force, the reference frame shown in fig.1 is defined for the two kinds of detector used for the measurement, i.e. the sensors placed in the Tracker Inner Barrel (TIB) layers, with an active thickness equal to $290\,\mu$m, and the others placed in the Tracker Outer Barrel (TOB) layers, with an active thickness of $500\,\mu$m [4]. The x coordinate of the hole path endpoints at the junction side of the detector, expressed not in terms of strips but as the actual distance (micron) from the origin of the reference frame, is then calculated. Assuming a track incident on the origin of the reference frame and forming an angle $\theta_{\rm t}$ with respect to the z axis (see fig.1), the x coordinate of the path endpoint at the junction

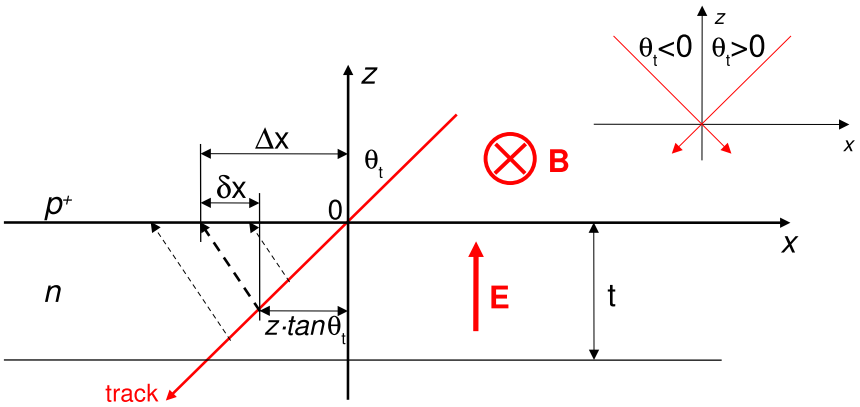

Figure 1: *Model for the hole Δx displacement due to the Lorentz force. The holes are freed by a traversing particle incident with an angle $\theta_{\rm t}$ with respect to the detector normal. On the top right the adopted conventions on the incidence angle signs are also shown.*

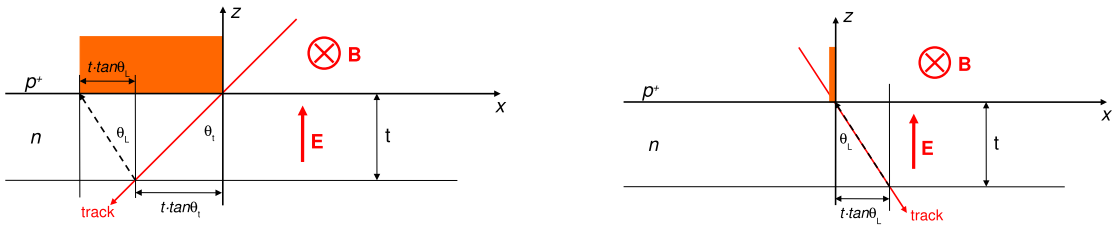

(a) (b)

Figure 2: *Cluster formation in presence of a magnetic field, with the approximations adopted for the model. Tracks incident with a generic angle (a) and with an angle equal to the Lorentz angle (b) are considered. The cluster is represented by the rectangle.*

side for a hole formed at depth $z\,(\leq 0)$ is given by:

$$\Delta x(z,\theta_t) = z\cdot\tan\theta_{\rm t} + \delta x(z)\,, \tag{2}$$

where $z\cdot\tan\theta_{\rm t}$ is the horizontal projection of the track and $\delta x(z)$ is the endpoint displacement due to the Lorentz force

$$\delta x(z) = -z\cdot\tan\Theta_L\,. \tag{3}$$

With the conventions on the axis and magnetic field sign adopted in fig.1, a negative sign for $\tan\Theta_L$ and for the hole displacement $\delta x(z)$ is expected. Thus the centroid of the cluster generated by the track is displaced by

$$\delta x_{\rm cluster} = \frac{t}{2}\cdot\tan\Theta_L\,, \tag{4}$$

with respect to the position in the absence of magnetic field, where t (positive) is the thickness of the sensor. If the displacement is measured, the Lorentz angle can be calculated as

$$\tan\Theta_L \equiv \frac{2\delta x_{\rm cluster}}{t}\,. \tag{5}$$

Measuring the displacement is however difficult as the expected value is order of few tenths of microns. Alternatively the Lorentz angle can be obtained from the cluster width versus $\theta_{\rm t}$, the track incidence angle in the plane orthogonal to the strips. In the absence of a magnetic field the hole drift follows the electric field lines, which are normal to the strips. Hence tracks orthogonal to the detector achieve a minimum cluster width. If the track incidence angle increases, the cluster size increases accordingly. On the contrary, in the presence of a magnetic field, the drift direction is no longer along the electric field lines, as shown in fig.2. Therefore the minimal cluster size is found for particles traversing the detectors with the same inclination as the drift lines. Since the angle between electric field and drift direction is by definition the Lorentz angle, the measurement of the track incident angle for which minimum cluster size is achieved provides a direct measurement of the Lorentz angle itself. With reference to eq.(2), the Lorentz angle is Θ_L such that

$$\Delta x(z,\Theta_L) = 0\,. \tag{6}$$

In silicon detectors, however, the electric field changes linearly with the depth z, due to the spatial charge present in the depleted region, and for highly segmented detectors it is given by [1]:

$$\begin{aligned} E(z) &= \tfrac{V_{bias}-V_{depl}}{t} + \tfrac{2V_{depl}}{t^2}(t+z) \quad \text{for} \quad V_{bias}\geq V_{depl}\,, \\ E(z) &= \tfrac{2V_{bias}}{w^2}(w+z) \qquad\qquad\quad \text{for} \quad V_{bias} < V_{depl}\,, \end{aligned} \tag{7}$$

where z (≤ 0 in the adopted reference frame) is the depth inside the sensor, t is the detector thickness, V_{bias} is the bias voltage, V_{depl} is the depletion voltage and w is the thickness of the depleted region in the case of not fully depleted detectors. In fig.3 the shape of the electric field inside a generic TIB(TOB) module is shown, together with the corresponding hole mobility, for the specific working conditions of the detectors used for the measurement (as will be shown in the following). Since the hole mobility depends on the electric field, the Lorentz angle, as defined by eq.(1), is not constant in the silicon bulk and the measurements as obtained from eq.(5) and eq.(6) may yield

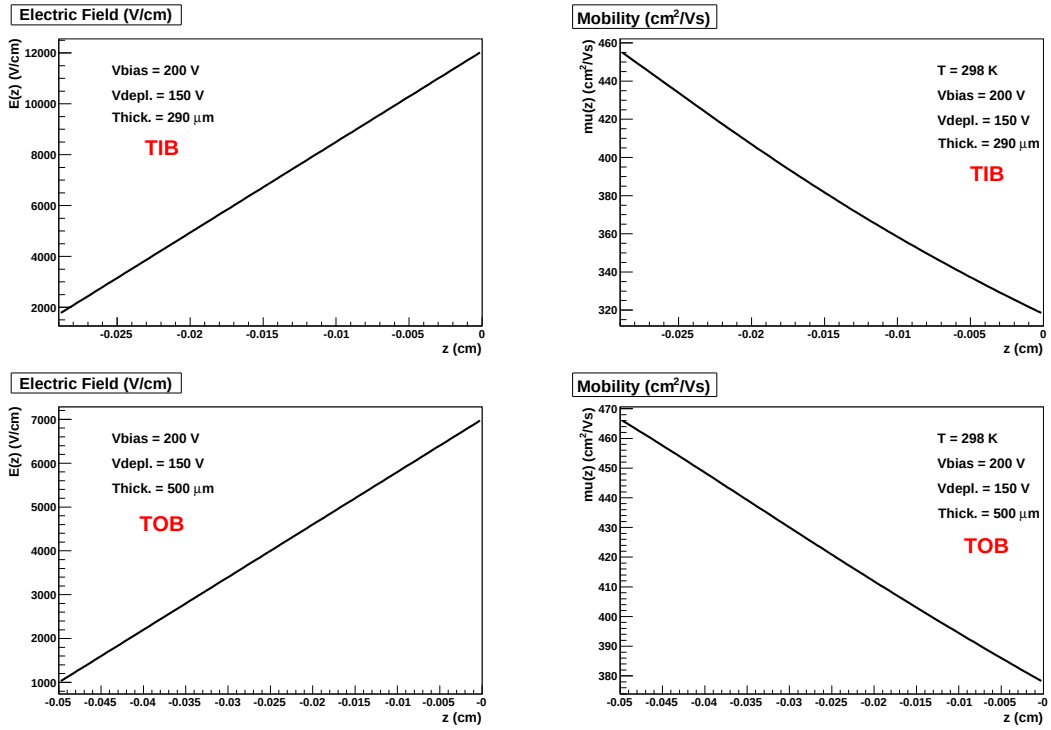

Figure 3: *Electric field (left) and hole mobility (right) inside a generic TIB(TOB) detector with* $V_{bias} > V_{depl}$.

different results. Though the most interesting result is related to the offset, as it is important to apply a correction for it when reconstructing an hit, the Lorentz angle is more easily obtained from the relation among the track angle and the cluster width, as already pointed out. For the present study, a numerical calculation developed to estimate the expected Lorentz angle, as obtained with both methods, in a wide range of detector operating conditions, is used.

The parametrization of the hole mobility used for the calculation is taken from [1]:

$$\mu(E) = \frac{\mu_{low}}{(1 + (\frac{\mu_{low} E}{v_{sat}})^{\beta})^{1/\beta}}\,, \tag{8}$$

where μ_{low} is the hole mobility for low electric fields, v_{sat} is the saturation drift velocity and β is a fit parameter. The following values for μ_{low}, v_{sat} and β are used for the holes [1]:

$$\begin{aligned} \mu_{low} &= 470.5(\mathrm{cm}^2/\mathrm{Vs})\left(\tfrac{T}{300\mathrm{K}}\right)^{-2.5}\,, \\ \beta &= 1.213\left(\tfrac{T}{300K}\right)^{0.17}\,, \\ v_{sat} &= 8.37\times 10^6(\mathrm{cm/s})\left(\tfrac{T}{300\mathrm{K}}\right)^{0.52}\,. \end{aligned} \tag{9}$$

Since TIB and TOB modules have different thicknesses, modules which have the same depletion voltage and the same bias voltage applied obviously have different electric field inside and hole mobility too. The effect of the magnetic field on the mobility is expressed by the Hall factor r_H, assumed 0.7 for holes at room temperature [1]. The endpoint displacement along the x coordinate for a hole created at depth z is given by:

$$|\delta x(z)| = r_H B \int_z^0 \mu(z')\mathrm{d}z'\,, \tag{10}$$

where B is the intensity of the magnetic field, $\mu(z)$ is the mobility and the sign of $\delta x(z)$ is negative, as stated before.

The model assumes an uniform energy loss to calculate the centroid of the cluster formed by the holes generated by the passage of the particle. To this purpose the detector is divided in n slices, each with a thickness equal to t/n and $\Delta x(z, \theta_t)$, as defined in eq.(2), is calculated for each slice. Thus the cluster position for a particle incident with an angle θ_t is obtained from the centroid of the charge as

$$x_{\mathrm{cluster}}(\theta_t, x_{\mathrm{track}}) = \frac{1}{t}\int_{-t}^{0} \Delta x(z, \theta_t)dz + x_{\mathrm{track}}\,, \tag{11}$$

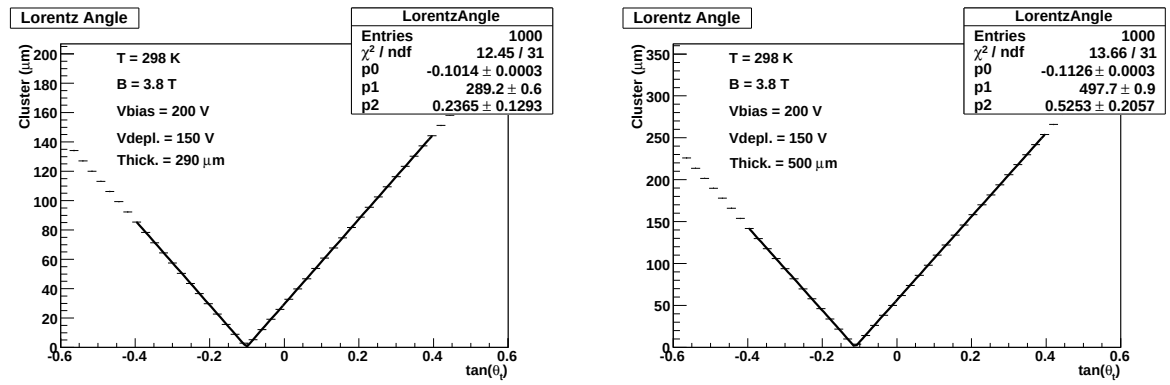

Figure 4: *Estimate of the tangent of the Lorentz angle (p_0) provided for the model, for TIB (left) and TOB (right) modules, at the MTCC working conditions.*

where $x_{\rm track}$ is the coordinate of the track intersection with the strip plane. The cluster size is obtained from the absolute value of the difference between the maximum and minimum x coordinate of the hole path endpoints ($x_{\rm max} - x_{\rm min}$). In case of a not fully depleted detector the calculation is limited to the depleted region.

As shown in fig.3, the hole mobility is nearly linear for the working conditions of the detectors used for the measurement, both for TIB and TOB modules. Deriving δx from eq.(10), however, allows one to consider a wide range of depletion voltages versus bias voltages, including cases where the detector is not fully depleted, a condition that can arise, for example, as a consequence of radiation damage.

In the model the carrier diffusion and the capacitive interstrip couplings are neglected. Actually both these effects contribute to the enlargement of the cluster size, but nevertheless, in first approximation, they do not change the position of the centroid of the collected charge, nor the track incidence angle corresponding to the minimum cluster width.

The model is used to calculate cluster position and sizes for various conditions of the magnetic field and detector parameters (i.e. depletion voltage, bias voltage and temperature) for tracks whose incidence angle spreads uniformly between -30° and $+30^\circ$.

In the case of model results, the search for the minimum can be done numerically. In real data, however, the average cluster width can be estimated with some statistical precision only for a range of track incidence angles, i.e. only a binned distribution can be obtained. To find the minimum therefore a fit to this distribution is necessary. The same procedure is followed on the data obtained from the model. The results are plotted as cluster size versus the tangent of the incidence angle. An example of this type of plot is given in fig.4 where it is evident that the minimum cluster size is achieved for a value of the incidence angle which is not zero anymore. Thus a fit on the histograms is performed using the following function:

$$p_1 \cdot |\tan\theta_{\rm t} - p_0| + p_2\,, \tag{12}$$

where the parameter p_0 represents the tangent of the Lorentz angle defined previously. A comparison with results obtained from a numerical search of the minimum of Δx showed no difference with the result of the fit using (12).

Using this model it is thus possible to estimate the Lorentz angle for the specific working conditions of the detectors at the moment of data taking during the MTCC. Moreover it is possible to estimate the a priori uncertainties which depend on the precision with which the detector parameters were known (detector temperature, depletion voltage, bias voltage and the intensity of the magnetic field in the tracker region).

Due to the low statistics available, it is not possible to consider each module separately, but aggregate data for each layer must be considered. Therefore the estimation of the Lorentz angle and its a priori uncertainty is obtained using values of temperature (T), depletion voltage (V_{depl}) and bias voltage (V_{bias}) consistent with all the modules used during data taking:

$$\begin{array}{lcl} T & = & (298 \pm 15)\,{\rm K}\,, \\ V_{depl} & = & (150 \pm 100)\,{\rm V}\,, \\ V_{bias} & = & (200 \pm 5)\,{\rm V}\,. \end{array} \tag{13}$$

The value of V_{depl} is the average of the depletion voltages of the modules, as measured before assembly. A few

Table 1: *Estimate of the a priori uncertainties on* $\tan\Theta_L$*, obtained by the model for TIB and TOB modules.*

	$\Delta(\tan\Theta_L)$ TIB	$\Delta(\tan\Theta_L)$ TOB
T = (298 ± 15) K	$^{+0.008}_{-0.011}$	$^{+0.011}_{-0.012}$
V_{depl} = (150 ± 100) V	$^{+0.002}_{-0.0004}$	$^{+0.001}_{-0.0001}$
V_{bias} = (200 ± 5) V	± 0.0005	± 0.0003
B = (3.80 ± 0.05) T	± 0.0012	± 0.0013

modules had $V_{depl} > V_{bias}$ during the measurement and thus were not completely depleted. On the other hand V_{bias} could not be increased more because some modules went in breakdown for bias voltages higher than 200 V. The modules used for MTCC in fact were not the ones which will be used for the final tracker, but pre-series modules of worse quality. Also the temperature of the modules varied considerably among the layers and among modules belonging to the same layer. A rough estimate of the temperature was given by the temperature of the cooling system liquid.

The value of the magnetic field in the detector region was [5]:

$$B = (3.80 \pm 0.05)\,\mathrm{T}\,, \tag{14}$$

where the error includes the uncertainty on the solenoid current, on the calibration and the uncertainty due to the dependence of the field intensity on the radial distance from the interaction point (the field dependence on the Z coordinate of the global reference frame was negligible because of the limited space occupied by the detectors along this direction).

The expected TIB(TOB) Lorentz angles, relative to the working conditions described above, are respectively:

$$\begin{aligned} &\textbf{TIB:} \quad \tan\Theta_L = -0.1014 \quad \Rightarrow \quad \Theta_L \simeq -5.8^\circ\,, \\ &\textbf{TOB:} \quad \tan\Theta_L = -0.1126 \quad \Rightarrow \quad \Theta_L \simeq -6.4^\circ\,, \end{aligned} \tag{15}$$

as shown in fig.4.

The a priori uncertainty is evaluated by performing the fit described above both for TIB and TOB modules, varying the values of temperature, depletion voltage, bias voltage and magnetic field within the uncertainties quoted in (13) and (14). Tab.1 summarizes the results. The most relevant contribution to the a priori uncertainty is given by the knowledge of the module temperature.

Thus the predicted Lorentz angle for the two kinds of detector used at the MTCC is

$$\begin{aligned} (\tan\Theta_L)^{\mathrm{TIB}}_{MTCC} &= -0.101 \quad {}^{+0.008}_{-0.011} \\ \Rightarrow (\Theta_L)^{\mathrm{TIB}}_{MTCC} &= -5.8^\circ \quad {}^{+0.5^\circ}_{-0.6^\circ}\,, \\ (\tan\Theta_L)^{\mathrm{TOB}}_{MTCC} &= -0.113 \quad {}^{+0.011}_{-0.012} \\ \Rightarrow (\Theta_L)^{\mathrm{TOB}}_{MTCC} &= -6.4^\circ \quad \pm 0.6^\circ\,. \end{aligned} \tag{16}$$

These values of Lorentz angle, if considered constant along the module thickness, would correspond to a displacement on the cluster centroid of approximately $15\,\mu$m for TIB and $27\,\mu$m for TOB modules, which is comparable to the intrinsic resolution of the microstrip detectors. The difference with respect to the calculation of the centroid of the charge is only 2-3 μm, therefore it can be neglected for all practical purposes.

3 Lorentz angle measurement using cosmic muons

3.1 Data Sample

The Lorentz angle was measured using the data samples acquired at the MTCC in the period of August 23-29/2006, when the tracker was placed at the "Point 5" facility (P5) at CERN. Nearly 120 runs were acquired with the global

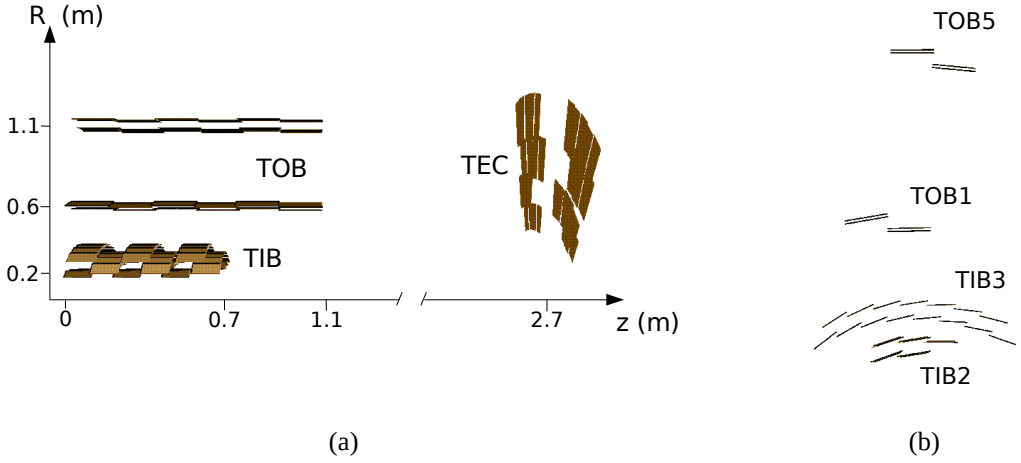

(a) (b)

Figure 5: *Layout of the tracker MTCC setup: (a) 3D view (the z axis and the radial coordinate of the global CMS reference frame are shown); (b) xy view of the barrel part. The instrumented parts are a fraction of layer 2 and layer 3 of TIB, two rods in layer 1 and in layer 5 of TOB, two petals in disk 9 of TEC.*

trigger provided by the muon chambers, with magnetic fields of 0T, 3.8T and 4T [3]. Nevertheless the 4T runs were not used for the measurement, because of the low statistics available for this particular value of the magnetic field. Moreover among the 0T and 3.8T runs acquired, were selected the ones that did not present any problem in the DAQ and for which a stable value of the magnetic field was reported.

The tracker setup for the MTCC is shown in Fig. 5. The active area of the MTCC tracker detector consists of 0.75 m^2 of silicon sensors. These were arranged in three basic structural units corresponding to the major subsystems of the CMS tracker: the Tracker Inner Barrel (TIB), the Tracker Outer Barrel (TOB) and the Tracker Endcap (TEC).

The TIB structure consisted of two mechanical prototype shells corresponding to layers 2 (L2) and 3 (L3) of the entire TIB: layer 2 contained 15 double-sided modules and layer 3 contained 45 single-sided modules. Four TOB sub-structures ("rods") were mounted in locations corresponding to layers 1 and 5 of the final TOB. The L1 rods each contained six single-sided modules with a strip pitch of 183 μm, and the L5 rods contained six single-sided modules with a strip pitch of 122 μm. Two TEC sub-structures ("petals"), each holding 17 silicon strip modules distributed in rings 4-7, equipping a custom-made disk, corresponding to disk 9 of the TEC, completed the MTCC tracker setup.

Since the angular acceptance of the muon chambers was much larger than the tracker volume, among all the triggered cosmic muons only very few yielded a signal in the tracker modules. For this reason an event filter was applied which selected those events with a muon also in the tracker barrel layers. The algorithm is based upon the presence of clusters in at least three out of the four different TIB and TOB layers. The fraction of filtered events with this algorithm was less than 10^{-3}. Unfortunately, because of the specific MTCC tracker layout, triggered muons could not cross simultaneously both TEC modules and either TIB or TOB layers. Therefore for TEC studies another event filter was required. However this fact is not relevant for the Lorentz angle measurement, since the magnetic field lines are nearly parallel to the electric field lines inside the TEC modules, and thus the charge carriers inside them are not affected by Lorentz deviation. Thus for this study events with tracks in the TEC modules are not considered. Due to the presence of some noisy modules in TOB layers, an additional filter is also applied that rejects reconstructed tracks which have a hit in the TOB layers with a charge of less than 80 ADC counts (the most probable value of the hit charge in TOB modules is about 160 ADC counts). The use of this additional filter improves the quality of the reconstructed tracks.

For this measurement, tracks reconstructed with two different algorithms were used, named "Cosmic Track Finder" (CTF) and "Road Search" (RS) algorithms [6]. Moreover the track reconstruction was performed using two different sets of alignment constants, both of them obtained by using a track-based alignment algorithm named "Hit and Impact Point" (HIP) [6]. The first set of alignment constants was obtained using survey information (i.e. measurements of the center points and orientations of the sensors) as starting point for the alignment procedure,

Table 2: *Analyzed data samples for $B = 0\,\mathrm{T}$ and $B = 3.8\,\mathrm{T}$. Number of tracks reconstructed using Cosmic Track Finder (CTF) and Road Search (RS) algorithm and the two alignment settings available. The clusterization thresholds used are: $t_{\mathrm{Seed}} = 4$, $t_{\mathrm{Channel}} = 3$ and $t_{\mathrm{Cluster}} = 5$.*

Magnetic field	#Events	#Filtered events
B=0.0 T	10 197 963	6 096
B=3.8 T	12 638 378	3 406

Magnetic field	#Reco. tracks - CTF al. with survey	#Reco. tracks - CTF al. without survey
B=0.0 T	5 299	5 295
B=3.8 T	2 989	3 104
Magnetic field	#Reco. tracks - RS al. with survey	#Reco. tracks - RS al. without survey
B=0.0 T	4 522	4 513
B=3.8 T	2 085	2 080

while the second one did not use this information. Thus the former will be named "alignment with survey" in the following, while the latter "alignment without survey". These two different settings of alignment constants were used to check the contribution to the error on the measurement due to the alignment itself.

In Tab.2 the total number of events acquired in the selected runs and the number of filtered events are reported. The standard clusterization thresholds are used [7], i.e. 4 noise sigma's for the seed (t_{Seed}), 3 for the nearby strips (t_{Channel}) and 5 for the total cluster charge (t_{Cluster}). The number of tracks reconstructed using the two available tracking algorithms and the two settings of alignment constants is also shown. The fluctuation of the number of reconstructed tracks (see CTF tracks at B = 3.8T) is probably due to fake tracks. The lower quality of the modules used for MTCC in fact yields many noisy hits with the standard thresholds of the clusterizer. This fact, together with other reasons that will be explained in sec.3.3, suggests an increase of the clusterization thresholds as will be described in the following.

3.2 Measurement method

The Lorentz angle measurement with the data is performed using the same procedure defined when introducing the model, i.e. the angle for which a minimum cluster size is found. For a non zero magnetic field the average cluster size in strips for tracks incident with an angle θ_t with respect to the detector normal is given by:

$$\mathrm{average\,cluster\,size} = \frac{t}{p} \cdot p_1 \cdot |\tan\theta_t - p_0| + p_2\,, \tag{17}$$

where t is the detector thickness, p is the pitch, p_0 is the tangent of the Lorentz angle and p_1, p_2 are coefficients expressing the carrier diffusion and the electronic cross-talk between nearby channels. Profile plots of cluster size versus the tangent of the track incident angle are made for each layer and the Lorentz angle measurement is derived from the fit with the function shown in eq.(17).

Due to the fact that the Lorentz angle measurement is performed on the aggregate data coming from all the modules assembled on each layer, a correction which takes into account the different orientation of the modules is necessary. In fact some modules had the y axis of the local reference frame parallel to the magnetic field while the others anti-parallel. This engenders two different signs of Θ_L. Following the adopted reference frame (fig.1), if $\hat{y} \cdot \mathbf{B} > 0$ the sign of Θ_L is negative, positive otherwise. Moreover only the component of the cluster centroid displacement orthogonal to the module strips is measurable by the detector. Therefore the measurable displacement of the cluster centroid in the stereo detectors is less than the one observed in the mono detectors for the same angle of incidence, because of their 100 mrad inclination with respect to the mono detectors. Consequently a smaller Lorentz angle is measured in the stereo detectors, as shown in fig.6. With reference to the figure:

$$\Delta x_m = \frac{\Delta x_s}{\cos\alpha}\,, \tag{18}$$

where α is the angle between the y axis and the magnetic field (assumed parallel to the strips of the mono detector)

and $\cos\alpha$ is given by

$$\cos\alpha = \frac{\hat{y}\cdot\mathbf{B}}{\parallel\mathbf{B}\parallel}\,. \tag{19}$$

Therefore, to correct the effect due to the inclination of the stereo module strips, the measured values of $\tan\theta_t$ are multiplied by $1/\cos\alpha$. This correction is also applied to mono detectors, for which $\cos\alpha = \pm 1$. The expected sign of Θ_L thus is always negative.

3.3 Preliminary measurements

First of all it was verified that in the histograms obtained for null magnetic field the minimum cluster size was at $\tan\theta_t = 0$ as expected. Unfortunately, while clear minima for TIB layer 2 and TIB layer 3 histograms were obtained, both for CTF and RS tracks and for the two alignment sets used, a clear minimum for TOB histograms was never obtained. In fact the data showed a rather flat central region, corresponding to a cluster size roughly equal to 2 strips. As an example in fig.7 the results obtained for tracks reconstructed with RS algorithm using the alignment with survey are shown.

To understand this anomaly the measurement on another data sample was performed, acquired with null magnetic field when the tracker was in an other CERN facility, named "building 186" (186bd), for the first commissioning procedures. This data sample in fact was taken with a different configuration of the front-end readout chip (APV [8]) parameters and with a different geometrical configuration of the trigger, which was not provided in this case by the muon chambers but by three plastic scintillators placed above and under the tracker layers [6]. The results of 186bd data analysis, obtained using RS tracks and the alignment with survey, are shown in fig.8.

Comparing the histograms obtained with P5 and 186bd data, it is evident in the latter the minimum value of the cluster size smaller than the one seen in the P5 histograms, and in particular the presence of clear minima is evident in the TOB histograms too. Since the anomalies in the TOB histograms for P5 data were present for all tracking algorithms and alignment settings used, they can be ascribed to changed APV parameters and trigger configurations from 186bd to P5 data acquisitions. As a matter of fact, the influence of capacitive coupling between nearby strips depends on the APV settings, while the orientation of the detectors used for trigger increases the charge released in the TIB(TOB) modules by the traversing particles. Indeed, using at P5 the muon chambers for the trigger, the acquired tracks had, for geometrical reasons, an incidence angle in the plane parallel to the strips much larger than that of the tracks acquired with the scintillators as trigger. Both effects contribute to the increase in the cluster width for P5 data, shown in fig.9, causing the flat central region in P5 TOB histograms.

Having attributed the absence of clear minima in the P5 TOB histograms to the factors described above, the measurements were repeated raising the thresholds of the clusterizer. In fact, by increasing these thresholds, strips

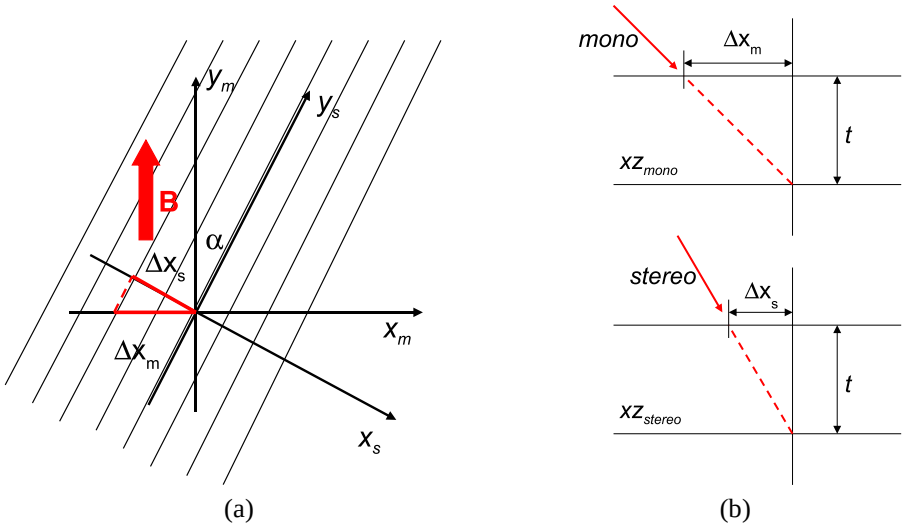

Figure 6: *Schematic representation of the Lorentz deviation in mono and stereo detectors; (a) junction side view: α is the angle between the stereo strips and the magnetic field (supposed parallel to the mono strips); (b) xz-mono and xz-stereo plane view: dashed lines represent the projection of the drift direction in the xz module plane, while the arrows represent the projection of the tracks which minimizes the cluster size.*

Table 3: *Analyzed data samples for $B = 0\,\mathrm{T}$ and $B = 3.8\,\mathrm{T}$. Number of tracks reconstructed using Cosmic Track Finder (CTF) and Road Search (RS) algorithm and the two alignment settings available with the new set of clusterization thresholds: $t_{\mathrm{Seed}} = 6$, $t_{\mathrm{Channel}} = 5$ and $t_{\mathrm{Cluster}} = 7$.*

Magnetic field	#Events	#Filtered events
B=0.0 T	10 197 963	5 888
B=3.8 T	12 638 378	3 304

Magnetic field	#Reco. tracks - CTF al. with survey	#Reco. tracks - CTF al. without survey
B=0.0 T	5 272	5 269
B=3.8 T	3 011	3 008
Magnetic field	#Reco. tracks - RS al. with survey	#Reco. tracks - RS al. without survey
B=0.0 T	4 463	4 456
B=3.8 T	2 069	2 064

with very low signals are removed and the cluster width thus becomes more sensitive to the track inclination. The measurement was performed using different configurations of the clusterizer thresholds, always maintaining the condition $t_{\mathrm{Channel}} < t_{\mathrm{Seed}} < t_{\mathrm{Cluster}}$. Finally the configuration for which the clearest minima were obtained without having an excessive decrease in the number of reconstructed clusters was chosen. This threshold configuration was: $t_{\mathrm{Seed}} = 6$, $t_{\mathrm{Channel}} = 5$ and $t_{\mathrm{Cluster}} = 7$. In Tab.3 the number of filtered events using these new clusterization thresholds and the number of reconstructed tracks are shown. The histograms obtained for each layer with the new clusterization thresholds are shown in fig.10, 11, 12 and 13. The 0T and 3.8T histograms are compared for each tracking algorithm and alignment settings used. Comparing in particular fig.7 and fig.12 it is evident the effect of changing the cluster thresholds, with the presence of clearer minima. In order to verify the stability of the fits, the ends of the fit range were varied by ± 0.02, i.e. by a quantity larger than the most significant error obtained on the fit parameters. In the worst case minima which differed from the ones provided by the fits by a quantity of the order of ~ 0.002 were obtained, i.e. lower than the statistical error.

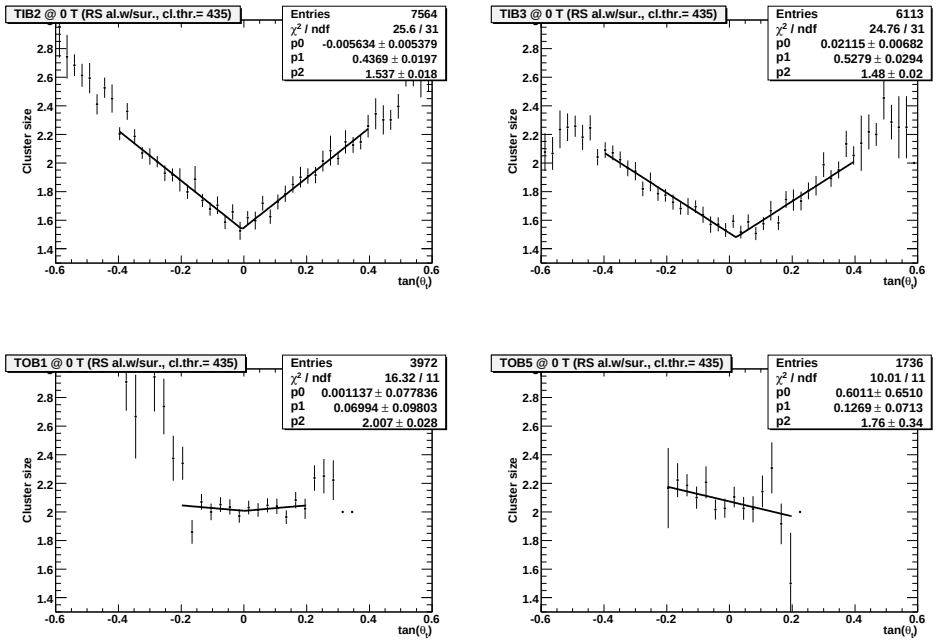

Figure 7: *Measurement of the cluster size minimization angle for 0* T *tracks acquired at P5. The measurements for TIB layers (upper plots) and TOB layers (lower plots) are shown. Road Search algorithm and alignment settings with survey information were used.*

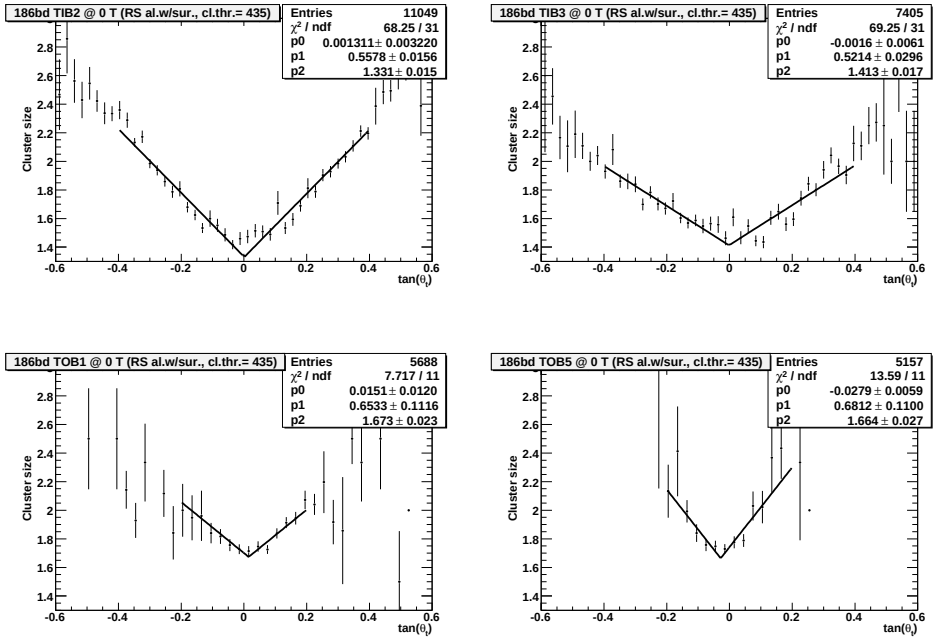

Figure 8: *Measurement of the cluster size minimization angle for 0* T *tracks acquired at 186bd. The measurements for TIB layers (upper plots) and TOB layers (lower plots) are shown. Road Search algorithm and alignment settings with survey information were used.*

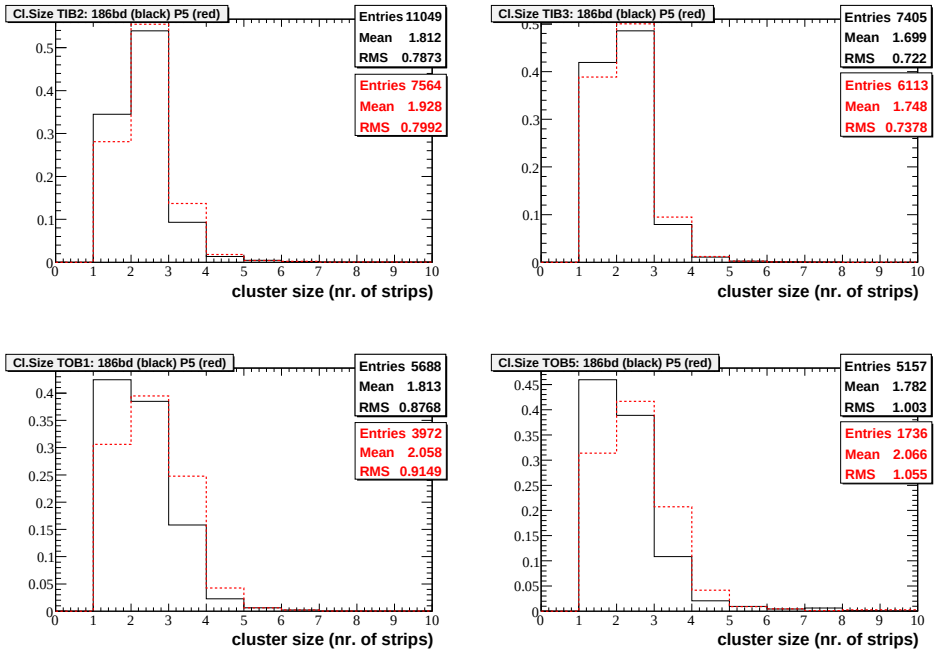

Figure 9: *Cluster size distributions normalized to the number of entries, for 186bd data (black solid line) and P5 data (red dashed line). The measurements for TIB layers (upper plots) and TOB layers (lower plots) are shown.*

3.4 Measurement results and uncertainties

To provide a correct estimate of the Lorentz angle, the value of p_0 obtained at 0 Tesla was subtracted to the one obtained at 3.8 Tesla, since a residual misalignment of the detectors can shift the measured value of $\tan\Theta_L$.

The correct estimate of the tangent of the Lorentz angle is then given by:

$$\tan\Theta_L = (p_0)_{3.8\mathrm{T}} - (p_0)_{0\mathrm{T}}\,, \tag{20}$$

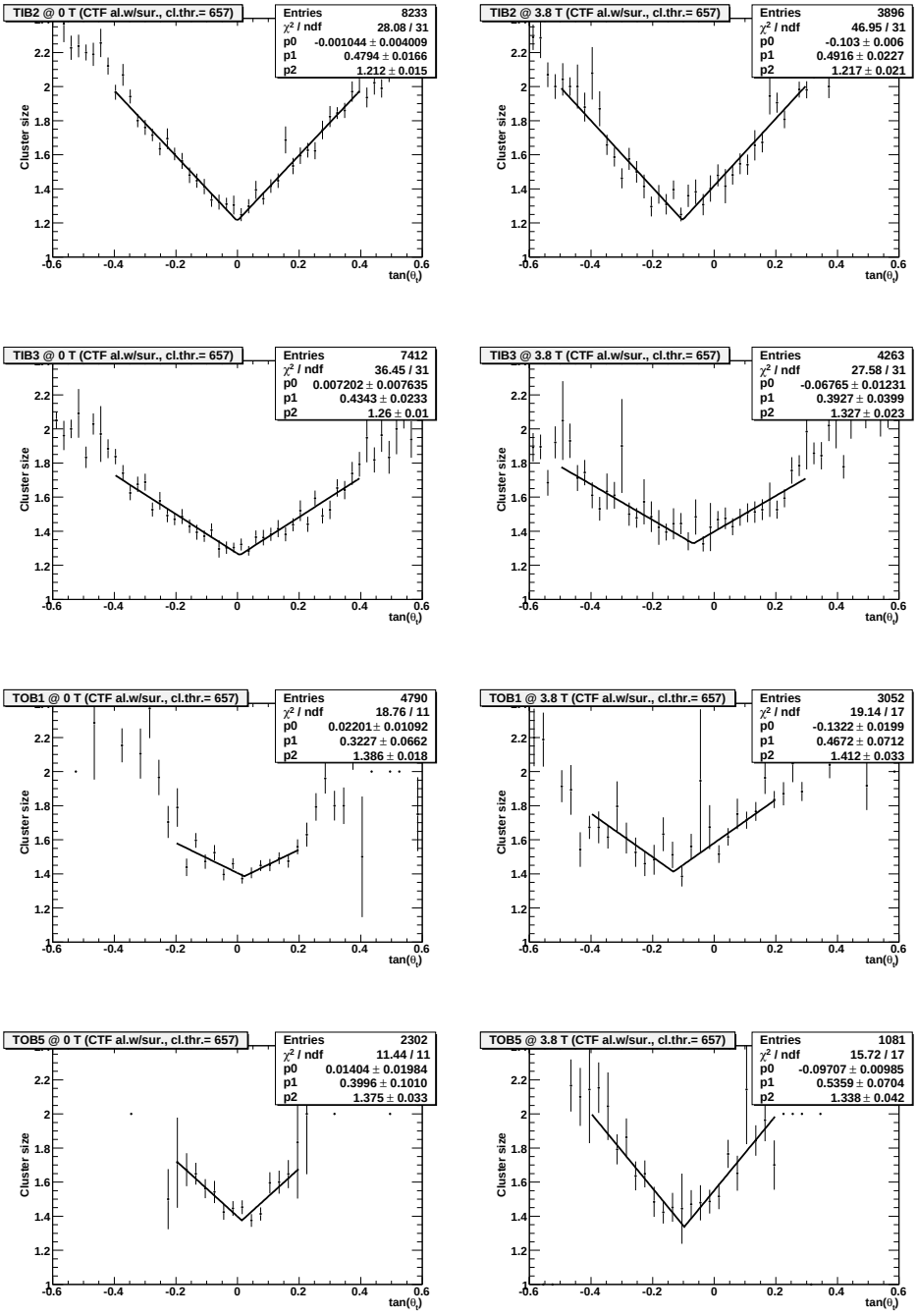

Figure 10: *Cluster size versus the tangent of the track incidence angle, at 0 T (left) and 3.8 T (right). The* (p_0) *parameter represents the tangent for which minimum cluster size is achieved. The measurement was performed on P5 data with clusterization thresholds:* $t_{\mathrm{Seed}} = 6$, $t_{\mathrm{Channel}} = 5$ *and* $t_{\mathrm{Cluster}} = 7$. *CTF tracks and alignment with survey were used.*

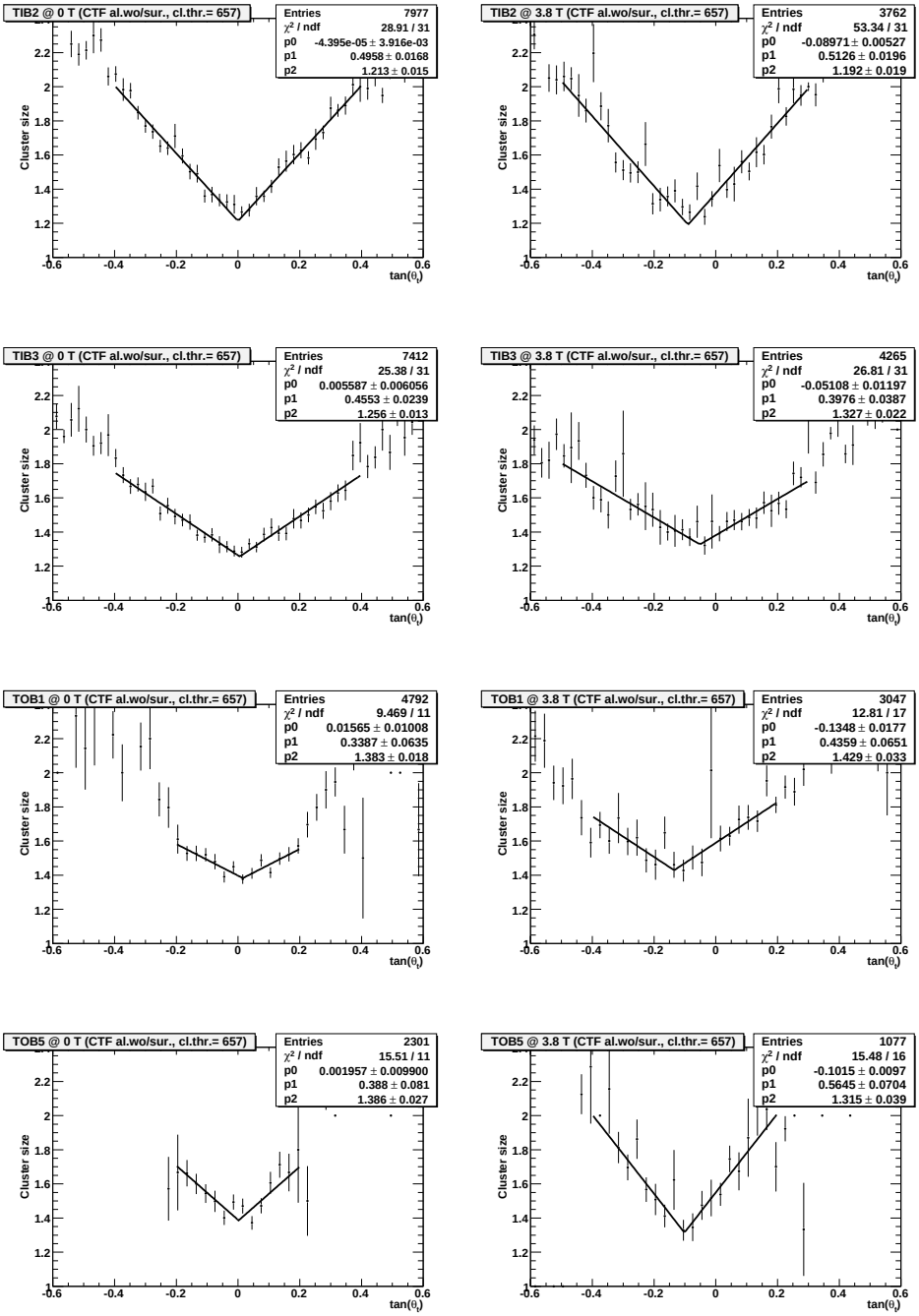

Figure 11: *Cluster size versus the tangent of the track incidence angle, at 0 T (left) and 3.8 T (right). The* (p_0) *parameter represents the tangent for which minimum cluster size is achieved. The measurement was performed on P5 data with clusterization thresholds:* $t_{\mathrm{Seed}} = 6$, $t_{\mathrm{Channel}} = 5$ *and* $t_{\mathrm{Cluster}} = 7$. *CTF tracks and alignment without survey were used.*

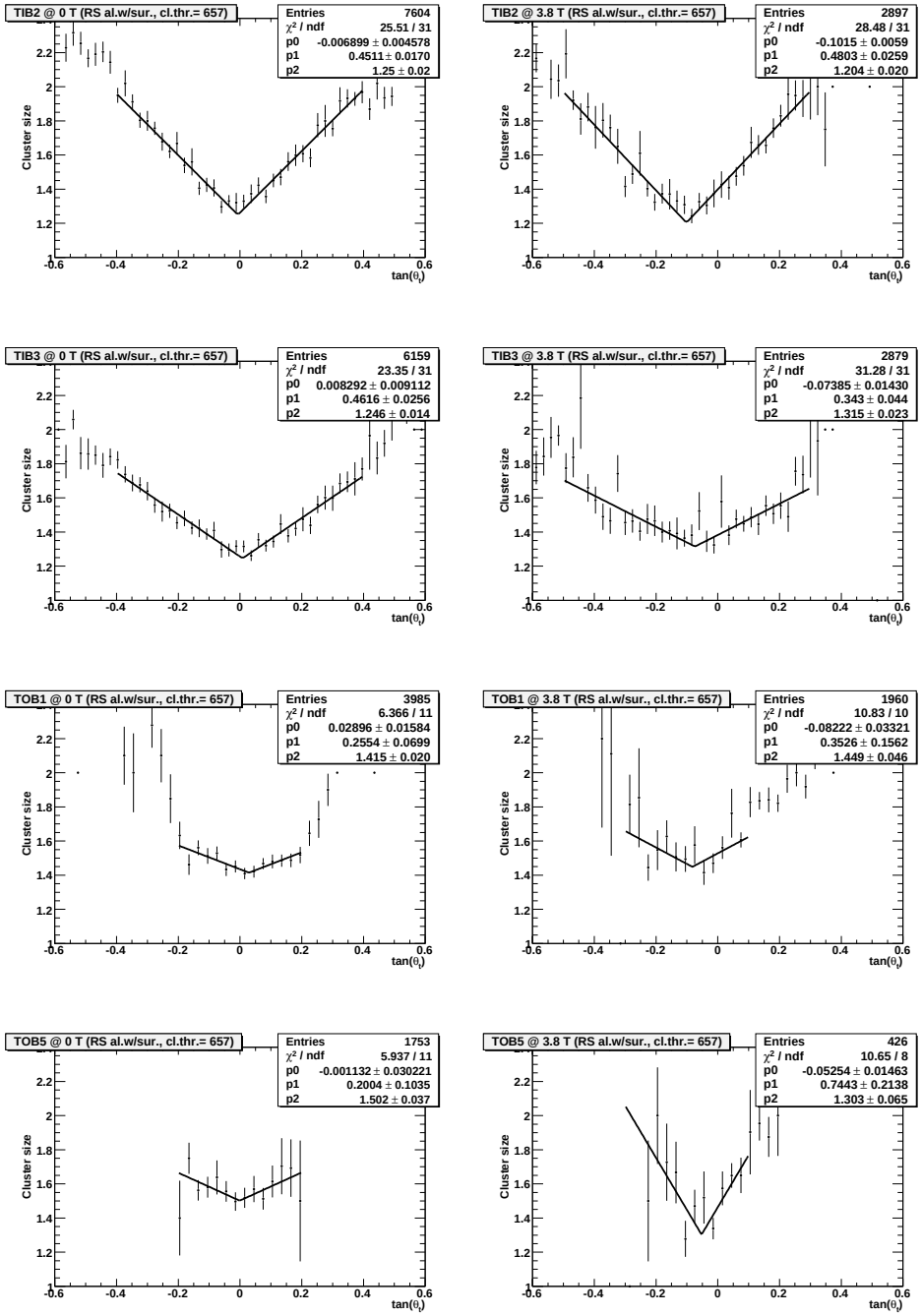

Figure 12: *Cluster size versus the tangent of the track incidence angle, at 0 T (left) and 3.8 T (right). The* (p_0) *parameter represents the tangent for which minimum cluster size is achieved. The measurement was performed on P5 data with clusterization thresholds:* $t_{\mathrm{Seed}} = 6$, $t_{\mathrm{Channel}} = 5$ *and* $t_{\mathrm{Cluster}} = 7$. *RS tracks and alignment with survey were used.*

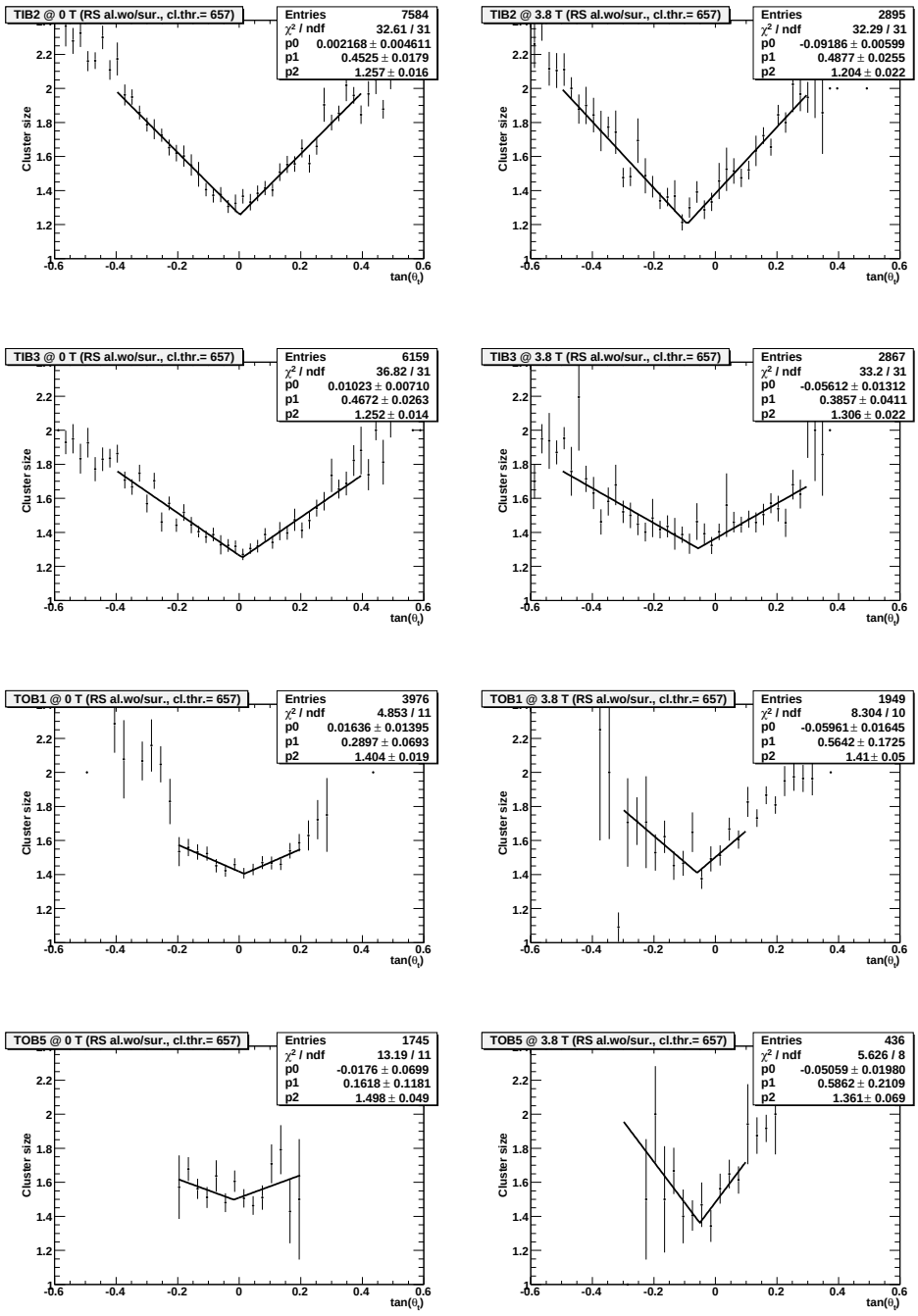

Figure 13: *Cluster size versus the tangent of the track incidence angle, at 0 T (left) and 3.8 T (right). The* (p_0) *parameter represents the tangent for which minimum cluster size is achieved. The measurement was performed on P5 data with clusterization thresholds:* $t_{\mathrm{Seed}} = 6$, $t_{\mathrm{Channel}} = 5$ *and* $t_{\mathrm{Cluster}} = 7$. *RS tracks and alignment without survey were used.*

Table 4: *Measured values of* $\tan\Theta_L$ *for B=3.8* T *in the four different layers.*

Layer	Measured $\tan\Theta_L$ Cosmic Track Finder	Measured $\tan\Theta_L$ Road Search
TIB Layer 2	-0.102 ± 0.007	-0.095 ± 0.007
TIB Layer 3	-0.075 ± 0.014	-0.082 ± 0.017
TOB layer 1	-0.154 ± 0.023	-0.111 ± 0.036
TOB layer 5	-0.111 ± 0.022	-0.051 ± 0.033

where $(p_0)_{3.8\mathrm{T}}$ and $(p_0)_{0\mathrm{T}}$ are the values of $\tan\theta_t$ corresponding to the minimum cluster size, obtained by the fits performed on 3.8 T and 0 T data samples respectively. The statistical uncertainty on $\tan\Theta_L$ is therefore given by:

$$(\Delta\tan\Theta_L)_{stat} = \sqrt{(\Delta p_0)^2_{3.8\mathrm{T}} + (\Delta p_0)^2_{0\mathrm{T}}}\,, \tag{21}$$

where $(\Delta p_0)_{3.8\mathrm{T}}$ and $(\Delta p_0)_{0\mathrm{T}}$ are the statistical uncertainties provided by the fits for $(p_0)_{3.8\mathrm{T}}$ and $(p_0)_{0\mathrm{T}}$ respectively. The results on $\tan\Theta_L$, obtained for the four different layers using the two available tracking algorithms and the alignment settings with survey information, are summarized in Tab.4.

As a check of the contribution to the error due to the precision of the alignment, the measurement described above was performed also using the alignment settings without survey information. The difference between the results obtained using the two sets of alignment constants is of the same order as statistical uncertainty (this can be seen from the plots in fig.10 to fig.13). The alignment error is also of the same order as the difference between the

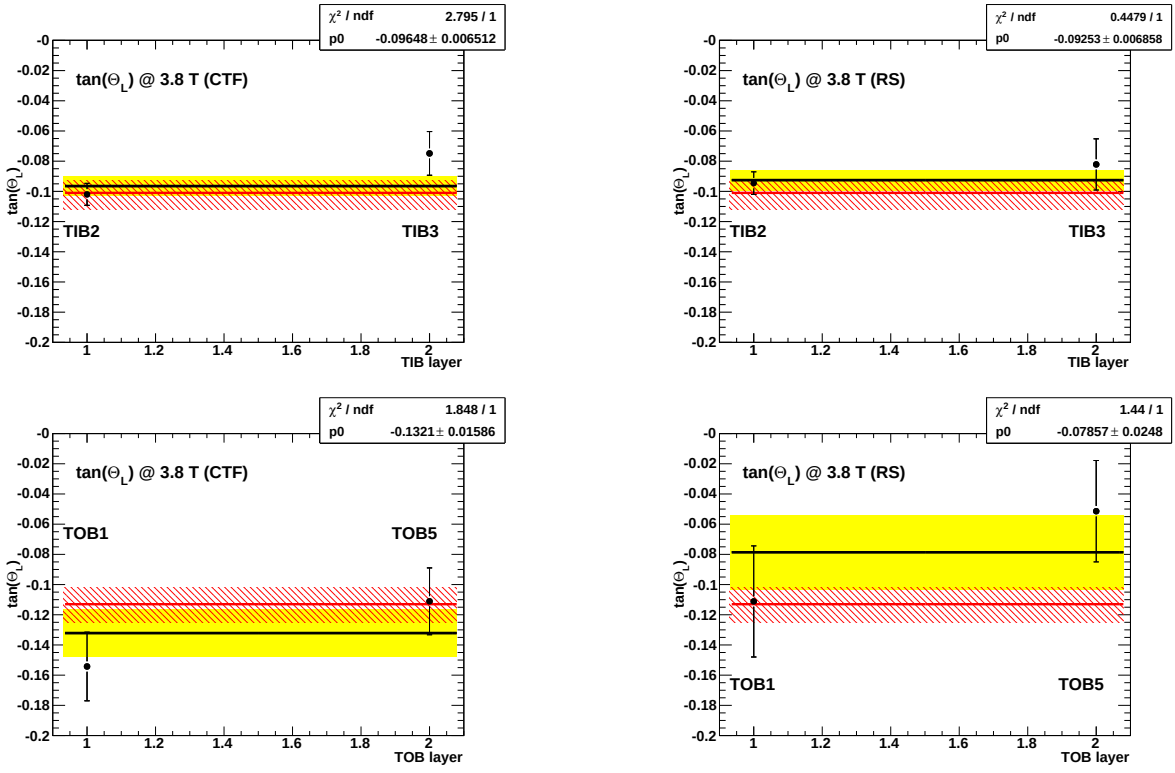

(a) (b)

Figure 14: *Results of the Lorentz angle measurement in the four different layers using tracks reconstructed by the Cosmic Track Finder algorithm (a) and Road Search algorithm (b). The black horizontal line represents the fit performed on the two TIB(TOB) layers and the solid band is the fit uncertainty. The red horizontal line represents the expected value together with its uncertainty (dashed band).*

Table 5: *Comparison between the measured values of the tangent of the Lorentz angle resulting from the fits, and the expected value. Results are shown both for Cosmic Track Finder and Road Search algorithm.*

	Measured $\tan\Theta_L$ Cosmic Track Finder	χ^2/n.d.f. CTF	Measured $\tan\Theta_L$ Road Search	χ^2/n.d.f. RS	Expected $\tan\Theta_L$
TIB value	-0.096 ± 0.006	2.8/1	-0.092 ± 0.007	0.4/1	$-0.101\ ^{+0.008}_{-0.011}$
TOB value	-0.132 ± 0.016	1.8/1	-0.079 ± 0.025	1.4/1	$-0.113\ ^{+0.011}_{-0.012}$

CTF and the RS final results. Thus in the absence of more precise estimation the systematic uncertainty due the alignment has been neglected.

To compare the measured values of $\tan\Theta_L$ shown in Tab.4 with the ones predicted by the model, the results obtained for TIB and TOB layers are plotted in separate graphs, since the model predicts two different values of $\tan\Theta_L$ for TIB and TOB modules. The results obtained with CTF and RS tracks are shown in fig.14, together with the results of the fits and the expected value with its a priori uncertainty. Tab.5 summarizes these results.

As shown in Tab.5 both the Cosmic Track Finder and the Road Search tracks yield a result in agreement with the expected value of the tangent of the Lorentz angle. The TOB results show a wider spread due to the relatively low statistics respect to the TIB. Since the χ^2 is lower using RS tracks the final estimate of the tangent of the Lorentz angle is derived using these reconstructed tracks.

4 Conclusions

The Lorentz angle in the CMS silicon microstrip detectors has been measured, for a 3.8 T magnetic field, on data collected during the Magnet Test and Cosmic Challenge. The cluster width versus the muon incidence angle was studied for events with 3.8 T magnetic field and without, from which the value of the Lorentz angle was extracted. The result was compared with the predictions from a model for the drift of the holes inside the silicon detector. The measurements, for the two kinds of detector used, yielded:

$$(\tan\Theta_L)^{\mathrm{TIB}}_{meas} = -0.092 \pm 0.007 \quad \Rightarrow \quad (\Theta_L)^{\mathrm{TIB}}_{meas} = -5.3^\circ \pm 0.4^\circ\,, \tag{22}$$

$$(\tan\Theta_L)^{\mathrm{TOB}}_{meas} = -0.079 \pm 0.025 \quad \Rightarrow \quad (\Theta_L)^{\mathrm{TOB}}_{meas} = -4.5^\circ \pm 1.4^\circ\,, \tag{23}$$

in agreement with the expected value of

$$\begin{aligned} (\tan\Theta_L)^{\mathrm{TIB}}_{exp} &= -0.101\ ^{+0.008}_{-0.011} \ \Rightarrow\ (\Theta_L)^{\mathrm{TIB}}_{exp} = -5.8^\circ\ ^{+0.5^\circ}_{-0.6^\circ}\,, \\ (\tan\Theta_L)^{\mathrm{TOB}}_{exp} &= -0.113\ ^{+0.011}_{-0.012} \ \Rightarrow\ (\Theta_L)^{\mathrm{TOB}}_{exp} = -6.4^\circ\ \pm 0.6^\circ\,. \end{aligned} \tag{24}$$

References

[1] V.Bartsch, W.de Boer, J.Bol, A.Dierlamm, E.Grigoriev, F.Hauler, S.Heising, L.Jungermann, *An algorithm for calculating the Lorentz angle in silicon detectors*, Nucl. Instr. and Meth. A 497 (2003) 389.

[2] I.V.Kotov, *Currents induced by charge collection in single side silicon microstrip detectors*, Nucl. Instr. and Meth. A 539 (2005) 267.

[3] CMS Note, *Tracker Operation and Performance at the Magnet Test and Cosmic Challenge*, CMS Note 2007/029 (2007).

[4] CMS Collaboration, *The Tracker Project Techincal Design Report*, CERN/LHCC 98-6, April 1998, CMS Collaboration, *Addendum to the CMS Tracker TDR*, CERN/LHCC 2000-016, February 2000.

[5] Martijn Mulders private communication.

[6] CMS note, *Tracking and Alignment with the Silicon Strip Tracker at the CMS Magnet Test Cosmic Challenge*, CMS Note 2007/030 (2007).

[7] CMS Collaboration, *Detector Performance and Software: Physics Technical Design Report*, Volume I, CERN/LHCC 2006-001 CMS TDR 8.1, February 2006, pg.240.

[8] M. Raymond et al., *The CMS Tracker APV25 0.25 μm CMOS Readout Chip*, 6th Workshop on Electronics for LHC Experiments, Cracow, Poland, September 2000.